Adaptive system of correction for the image jitter using a modified correlation sensor

L.V. Antoshkin, N.N. Botygina, O.N. Emaleev, P.G. Kovadlo,[1] P.A. Konyaev, V.P. Lukin, and V.V. Lavrinov

Institute of Atmospheric Optics, Siberian Branch of the Russian Academy of Sciences, Tomsk
[1] Institute of Solar-Terrestrial Physics, Siberian Branch of the Russian Academy of Sciences, Irkutsk

Received October 5, 2005

The results of testing the adaptive optics system with a correlation sensor at the Big Solar Vacuum Telescope at the Baikal Astrophysical Observatory are presented. Based on fast 12-bit DALSTAR DS-12-16K5H camera and an active mirror with a piezoelectric drive a system to correct for image jitter has been built, that shows good performance in the image patterns with 10 to 15% contrast. In tracking objects with a very noisy granulation image with 1 to 2% contrast, a modified correlation-tracking algorithm is proposed, which demonstrates a capability of using the correlation method in the case of low contrast objects.

Introduction

The adaptive optics systems intended for correction for image jitter are traditionally based on correlation algorithms.[1] At the Institute of Atmospheric Optics SB RAS, we have developed a prototype of such a system for use with the Big Solar Vacuum Telescope (BSVT) of the Baikal Astrophysical Observatory. The results reported in Refs. 2 to 4 demonstrate quite high efficiency of the correlation sensors in the case of tracking objects with 10 to 15% contrast.

In this paper, we discuss some new results obtained during our expeditions in 2003–2004 on the operation of the tracking system in studying low contrast objects like granulation pattern fragments. The experiments carried out at the BSVT and subsequent processing of the data obtained using high-speed photography (490 frames/s) with the use of a modified correlation tracking algorithm demonstrate the applicability of the correlation technique for processing the obtained results.

Instrumentation and measurement technique

Optical arrangement of the experimental setup at the BSVT is shown in Fig. 1. The modifications of the original setup (see Refs. 3 and 4) have mainly been done in the unit of optical signal recording. The image was captured with a 12 bit/pixel DALSTAR DS-12-16K5H camera with the frame grabbing rate of 490 frames/s. Frame grabbing was performed with a PC-DIG video signal controller through an RS-232 interface. Dark current of the first row of the CCD array was exposed to light and thus the row was ignored in measurements.

The software consisted of a utility tuning program and the main control program. The control program in its turn had several operation modes: measurement, tracking, and grabbing.

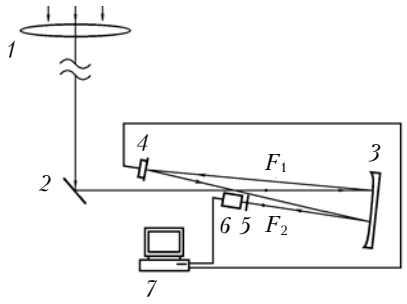

Fig. 1. Optical arrangement of the setup: telescope objective *1* (D = 760 mm, F = 40 m); beam-folding mirror *2*; spherical mirror *3* (F = 4 m); tip-tilt mirror *4*; filters *5*; DALSTAR video camera *6* (128×128 pixels, 12-bit ADC, 490 frames/s); computer *7* (Pentium VI, 2.4 GHz with a PC-DIG video card).

Before starting the experiment, in order to determine the feedback coefficient of the correlation tracker, we first determined the static characteristics of the tracker with the open control loop. For this purpose, a point source was placed at the telescope focus F_1 (see Fig. 1), the control signal was sent from the computer to the tip-tilt mirror *4*, and displacement of the point source image at the focus F_2 was measured with the correlation detector of image displacement.

When the main program run in the measurement mode, the stream of frames from the video camera was reproduced in the overlay window of the frame grabber driver. The correlation detector of image displacement yielded the results in real time in both digital and printed forms.

0235-6880/05/12 969-06 $02.00

In the tracking mode, the control signals came through the RS-232 drive controller to the piezoelectric drive for a tip-tilt control of the angular position of the mirror *4* (thorough description of the electronic unit and construction of the mirror with the piezoelectric push-bars can be found in Ref. 2).

The capture mode was intended for a fast recording and saving of a video signal to computer memory for its subsequent processing. Realizations of 1000 and 2000 frames, 128×128 pixels each, in a 16 bit/pixel format were first recorded to the main memory and then to the hard disc.

The operation of the adaptive system was evaluated using two parameters:

– the relative tracking error: σ_{er}/σ_c, where σ_{er} and σ_c are the rms deviations of the error and control signals;

– effectiveness of suppression of the spectral components of image jitter:

$$|S(f)|^2 / |S(f)_{er}|^2,$$

where $|S(f)|^2$ and $|S(f)_{er}|^2$ are the spectral power densities of the image displacement signals at an open control loop and residual image displacement signals in the tracking mode.

The correlation technique of measuring the image fragment displacements consisted in the following:

– at the start time, the reference frame I_R was stored, which then was used for calculation of the normalization array C_R;

– then, the normalized correlation function C_N of brightness distribution of the reference and current frames was calculated. Position of the peak of the correlation function determined the coordinates of the displacement of a current frame with respect to the reference one.

The calculations were performed by the following formulas: the correlation function

$$C(i,j) = \sum_{l=0}^{N-1} \sum_{m=0}^{M-1} I(l,m) I_R(i+l, j+m);$$

the normalized correlation function

$$C_N = C / C_R,$$

$$C_R(i,j) = \left[\sum_{l=0}^{N-1} \sum_{m=0}^{M-1} I^2(l,m) \sum_{l=0}^{N-1} \sum_{m=0}^{M-1} I_R^2(i+l, j+m) \right]^{1/2}.$$

To speed up the computations of the correlation function, we used the Fast Fourier Transform (FFT) algorithm:

$$C = F^- \left\{ F^+[I] F^+[I_R] \right\}.$$

We used the Mix Radix modification of the FFT algorithm, which allowed us to flexibly vary the size of the correlation analysis window and thus to obtain the desired speed of the tracking system operation.

To extend the applicability of the correlation technique and use it for tracking faint-contrast objects, we have proposed a modified FFT for calculating the correlation function:

$$C_m = F^- \left\{ F^+[I] F^+[I_R] H_B(k_x, k_y) \right\}.$$

The filtering function was set as a Gaussoid shifted with respect to the point of origin in the plane of spatial frequencies:

$$H_B(k_x, k_y) = \exp\left(-a[(k_x - k_{x0})^2 + (k_y - k_{y0})^2] \right).$$

Based on the experimental conditions, the filtering parameters were specified to provide the required sharpness of the correlation function peak.

Results

Tests of the correlation tracker at the BSVT performed in August, 2003, with a standard correlation detector based on an 8-bit DALSA CA-D1 video camera showed quite high efficiency of the system, when the object of tracking was an image fragment with a high contrast (10–15%) pore or a group of pores. Figure 2 shows the power spectra of image displacement signals at a closed (curve *2*) and open (curve *1*) control loop. At the same time, with a fragment of the granulation pattern, we did not manage to obtain such a result.

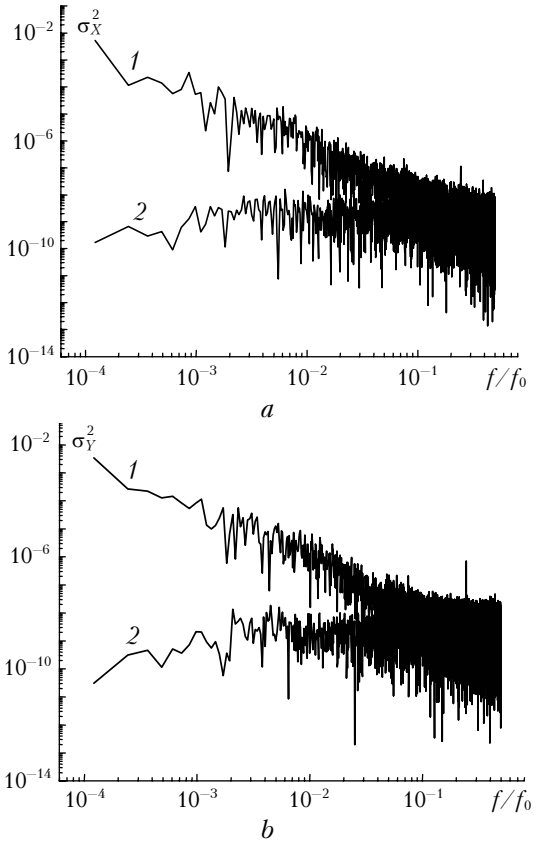

Fig. 2. Power spectra of the image displacement signals along the axes X (*a*), Y (*b*); f_0 = 164 Hz; duration of realization is 50 s; σ_{X1}/σ_{X2} = 36.0; σ_{Y1}/σ_{Y2} = 29.0.

Tests of the correlation tracker at the BSVT performed in August, 2004, with a standard correlation detector based on a 12-bit DALSTAR DS-12-16K5H video camera showed the same results. The reason of such a behavior of the detector is that the CCD-array of the DALSTAR video camera has four equidistant horizontal strings of elements, whose sensitivity is 0.4–1.2% lower than that of other elements. This results in appearance of four lines in the image under study. The contrast of these lines at a uniform illumination of the array is 0.2 to 0.6%.

In the correlation analysis of the images, the presence of fixed-position lines causes the appearance of a fixed local peak of the correlation function. In detection of low-contrast objects, it can happen that the value of a fixed local peak is higher than that in the image connected with the displacements. In this case, the detector does not record the displacements.

As known,[5] if the effect of atmospheric turbulence is ignored, the contrast of solar granulation in the central part of the Sun disc will lie with a high probability in the interval of 16 to 19%. The contrast is defined as the rms deviation of the brightness distribution normalized to the averaged brightness. If we assume the solar photosphere to be a black body, then this contrast should correspond to the rms deviations of the temperatures of 195 and 233 K at the average temperature of 5900 K. However, the atmospheric turbulence and instrumental errors dramatically reduce the contrast of the granulation pattern. Transfer of image, using additional optical elements, to the second focus in real telescopes with the correlation tracker also reduces the contrast of the granulation pattern.

Under the experimental conditions of 2003 and 2004, the contrast of the granulation pattern in different parts of the Sun disc (at its center, at the edge, and near sunspots) is on average in the interval from 1 to 4%. According to Ref. 6, this corresponds to the distribution of atmospheric turbulence, which is characterized by the Fried radius from 2 to 6 cm. To illustrate this, in Fig. 3 we present a diagram of the contrast of a series of frames at a two-second realization obtained with a 490 frames/s frequency. Changes in the image contrast for such a short time are connected with the turbulent and instrumental blur and displacement of the image rather than with the processes in the Sun.

During our 2004 expedition to the BSVT, we used a DALSTAR DS-12-16K5H video camera served as a receiver in the correlation detector and shot films on solar granulation for different parts of the Sun. This was done under conditions of clear sky at varying wind speed and visibility (as far as it was possible within the duration of the expedition). The films were made both in the primary and the secondary foci. We changed the receiver field of view, angular scale of the elements of the receiver matrix, and diameter of input aperture of the telescope. With the use of an additional optical element, in one frame we superposed two image fragments: the fragment with a pore, whose displacement is reliably measured with a correlation detector, and a fragment of the granulation pattern.

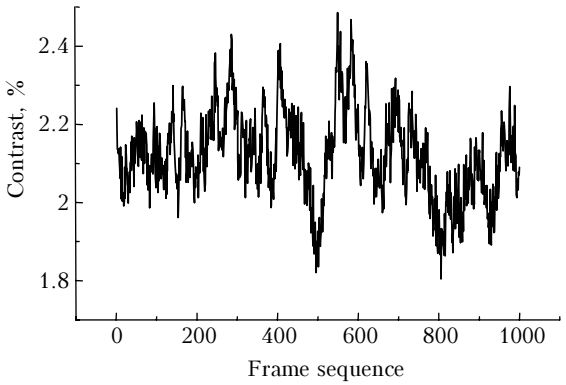

Fig. 3. The contrast of the solar granulation image near the spot in the primary telescope focus. Field of view of the receiver is 29×29 seconds of arc.

From the analysis of the recorded films, we had information on contrast and spatial scales of the structure of the granulation pattern in the form of the correlation function. The films helped us to verify the algorithms of correlation detector operation. In recording the displacement of the granulation pattern, we noticed that the correlation function of the reference and current frames had several extremes including fixed ones connected with the special features of the optical receiver. To separate the correlation function peak, whose coordinates determine the displacement of the granulation pattern, we used modification of the correlation algorithm. In the spatial spectra of the images of reference and current frames, the highest intensity was recorded at the frequencies of the size of the grains. The intensification contour had the form of the Gaussoid, whose parameters were specified separately for each fragment of the granulation pattern recorded.

Thus, the properly specified parameters resulted in suppression of low frequencies in the spatial spectrum, which smoothed the brightness over the detector filed of view, and high frequencies connected with the defects in the receiver array. Thus, the correlation function had a more pronounced peak connected with the displacement of the solar granulation image.

The use of films made it possible to develop criteria for selecting the parameters of the best intensification contour. To check correctness of a displacement measurement made with the modified correlation detector (MCD), this measurement was compared with the measurement data obtained with the traditional correlation detector (TCD). Only those image fragment displacements were measured, which

were well fixed with the traditional correlation detector.

Figure 4 shows a fragment of the Sun disc image, and Figs. 5–7 illustrate processing of this fragment with the TCD and MCD. The spot has a contrast of 21%. The film was recorded with a speed of 490 frames/s. We have analyzed displacement in 1000 frames. The root-mean-square deviations of the image displacement signals measured with the MCD were equal to 0.720 arc. s (along the X axis) and 5.121 (along the Y axis), and those measured with the MCD were, respectively, 0.720 and 5.119 arc. s. The film was shot on August 3, 2004, under strong wind conditions. In the image jitter spectrum, we observed a peak at a frequency of 7.6 Hz connected with vibrations of the siderostat mirror about the support axis.

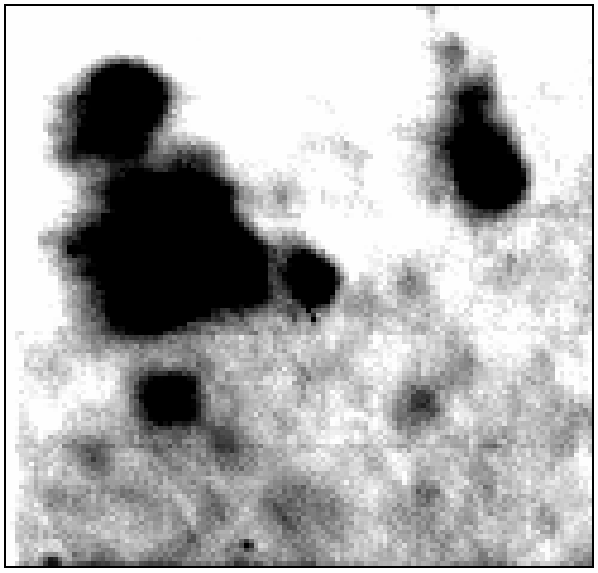

Fig. 4. Fragment of the Sun disc image corresponding to the field of view of 38×38 arc. s.

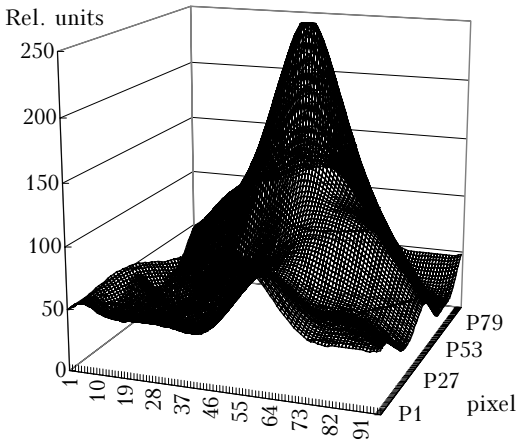

Fig. 5. Shape of the correlation function. The X- and Y-components are pixels, and the Z-component is values of the correlation function expressed in relative units.

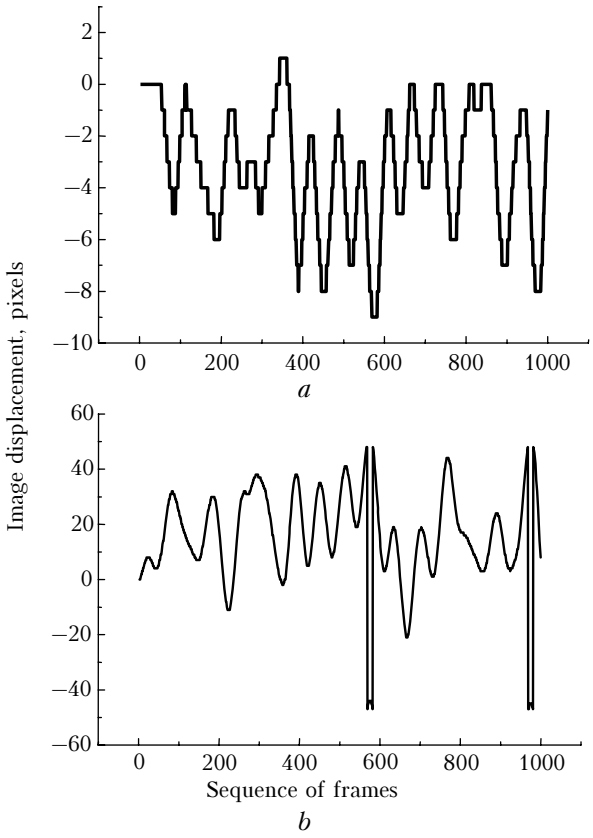

Fig. 6. Image displacements in the X- (a) and Y-directions (b) measured with the TCD (1 pixel = 0.3 seconds of arc.).

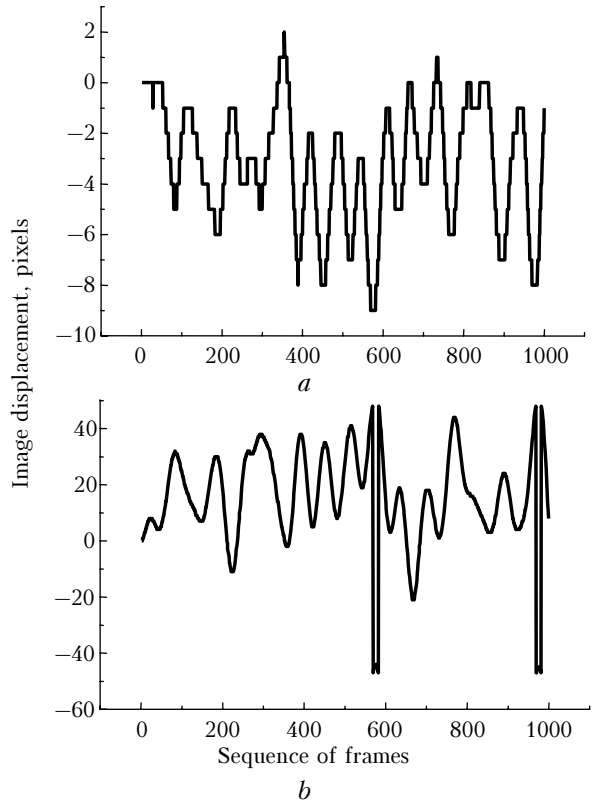

Fig. 7. The MCD-measured image displacements on the X (a) and Y (b) axes (1 pixel = 0.3 seconds of arc.).

Figure 8 shows a fragment of the granulation pattern, which the TCD has identified only poorly. The measured values of the contrast are given in Fig. 3. During realization, the contrast of the granulation pattern varied within 1.8 to 2.5%, the mean contrast was about 2.1%.

The correlation functions of the TCD and MCD are shown in Fig. 9. With the traditional correlation detector, the peaks of the correlation function connected with the fixed-position and displacing image structures are close in their values. The detector either reads "0" or tracks image movements. The correlation function of the MCD has a pronounced peak, which moves with the image motion.

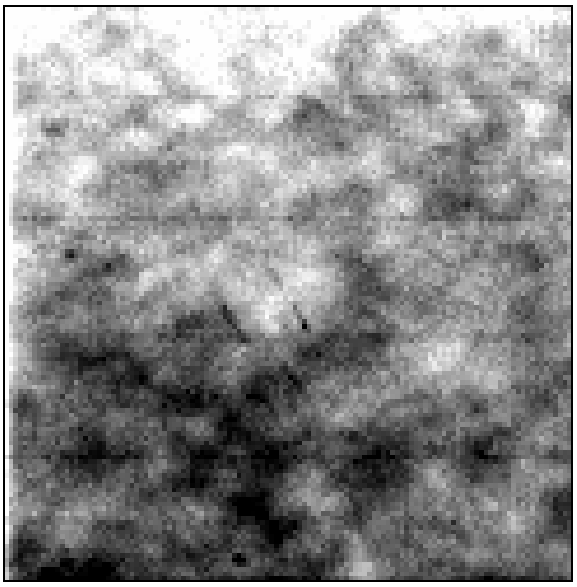

Fig. 8. Fragment of the granulation pattern.

In Fig. 10, we have illustrated the image displacement signals detected with the TCD (curve *1*) and MCD (curve *2*). The root-mean-square deviations of the image displacement signals measured with the MCD are equal to 1.350 seconds of arc. (on the X axis) and 4.490 seconds of arc (on the Y axis). The values obtained well agree with the corresponding values of the preceding realization (see Figs. 6 and 7). The time interval between the considered realizations is nine minutes.

In order to evaluate the capacities of the proposed modified algorithm of correlation tracking, we obtained distributions of the intensity of granulation pattern by averaging the sequence of 1000 frames.

Figure 11*a* shows the reference frame that corresponds to the time moment 0.002 s, where we can clearly see the granulation pattern of the Sun disc fragment. Because of strong transverse image vibrations, the resulting average image intensity for the time interval of 2 s is strongly dithered (Fig. 11*b*).

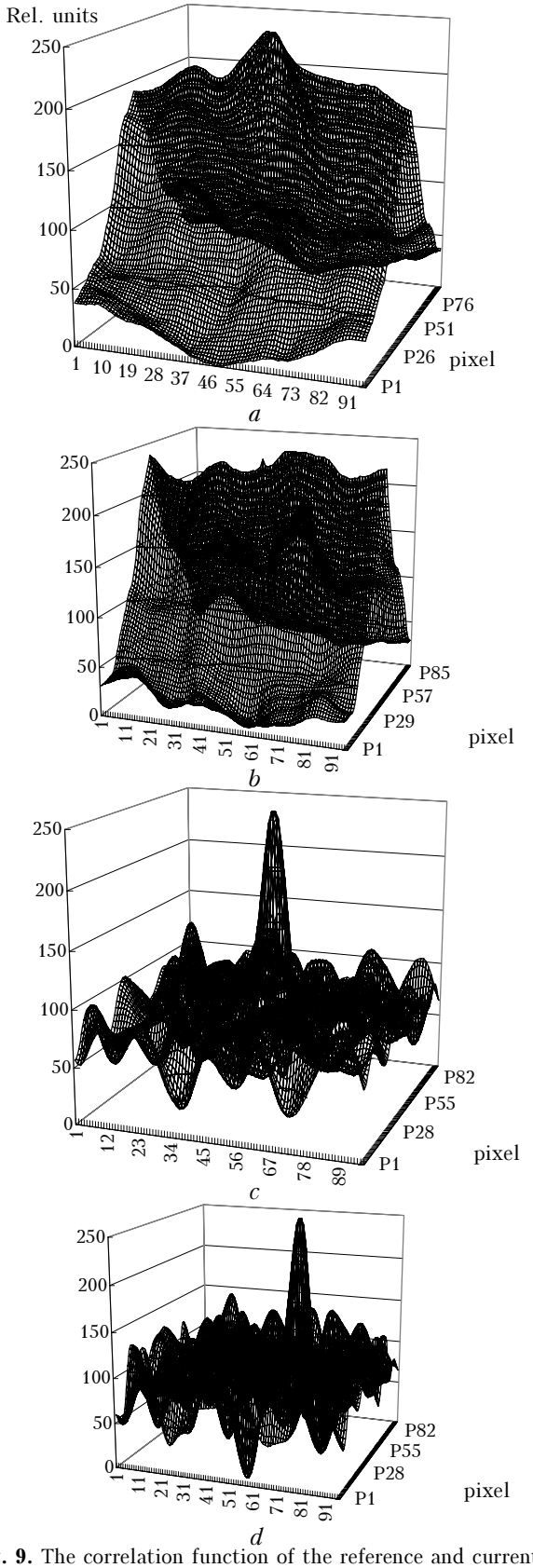

Fig. 9. The correlation function of the reference and current (10th (*a*, *c*), 306th (*b*, *d*)) frames captured with the TCD (*a*, *b*) and MCD (*c*, *d*). The X- and Y-components are pixels, and the Z-component shows the values of the correlation function expressed in relative units.

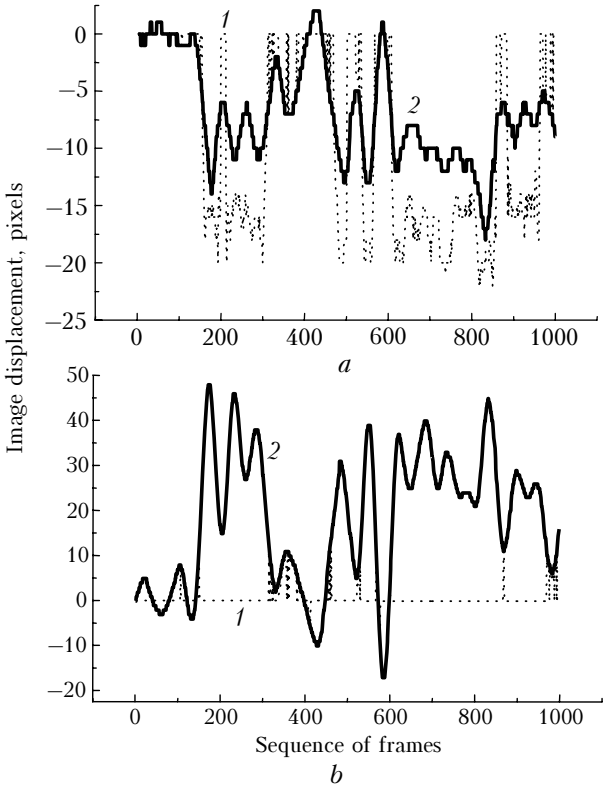

Fig. 10. Image displacements on the X (*a*) and Y (*b*) axes (1 pixel = 0.3 arc. s).

At the same time, in the tracking mode it was possible to restore the granulation structure (Fig. 11*c*) and thus to use the MCD in adaptive correction for the jitter of images with low-contrast objects.

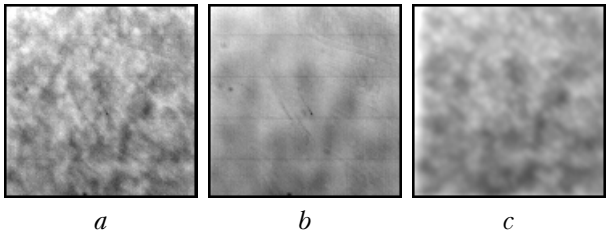

Fig. 11. Frames with the granulation pattern obtained in a *short exposure* mode (2 ms) (*a*); in a *long exposure* mode (2 s) without control (*b*); in a *long exposure* mode (2 s) with the modified correlation detector (*c*).

Conclusions

The tests of our adaptive optics system with the correlation detector performed in 2003–2004 at the BSVT of Baikal Astrophysical Observatory have proved a high efficiency of the system in tracking mage fragments with 10 to 15% contrast. If the object of tracking is a fragment of the granulation pattern with a contrast of 1–2%, the standard correlation detector stops functioning. In these cases, i.e., when modulation depth of the signal is only slightly greater than the noise modulation, application of the modified algorithm of correlation detector operation allows the detection of displacements of low-contrast image fragments to be performed.

In the Table, we have summarized the main characteristics of the adaptive system of image jitter correction developed for use at the Big Solar Vacuum Telescope. For comparison, we have also included here the parameters of other systems existing today throughout the world.

Parameter	USA	France	Spain	China	Russia, BSVT
	1989	1995	1996	2001	2003–2004
Telescope diameter, mm	760	900	980	430	760
Object of tracking	Granulation	Granulation	Granulation	Sunspot/pore	Pore/granulation
Algorithm	Cross-correlator		Absolute differences		Modified correlator
Sampling rate, Hz	417	582	1350	419	164–245
Field of view, arc. s.	10×10	2×2 ~ 12×12	14×14	5×5 ~ 20×20	33×33
Frequency band, Hz	25	60	100	84–30	120
Correction quality (rms, seconds of arc.)	0.023	0.02	0.05	0.14	0.07

Acknowledgments

The work has partly been supported by the complex integration project of Siberian Branch of the Russian Academy of Sciences "Modern Adaptive Telescope" (2003–2005).

References

1. O. Von der Luhe, A.L. Widener, Th. Rimmele, G. Spence, R.B. Dunn, and P. Wiborg, Astron. Astrophys. **224**, No. 2, 351–360 (1989).
2. L.V. Antoshkin, N.N. Botygina, O.N. Emaleev, P.A. Konyaev, V.P. Lukin, and A.P. Yankov, Prib. Tekh. Eksp., No. 1, 144–146 (2002).
3. L.V. Antoshkin, N.N. Botygina, O.N. Emaleev, P.G. Kovadlo, P.A. Konyaev, V.P. Lukin, A.I. Petrov, and A.P. Yankov, Atmos. Oceanic Opt. **15**, No. 11, 934–937 (2002).
4. L.V. Antoshkin, N.N. Botygina, O.N. Emaleev, V.M. Grigoriev, P.A. Konyaev, V.P. Lukin, P.G. Kovadlo, V.I. Skomorovskii, and A.P. Yankov, Avtometriya **39**, No. 5, 77–89 (2003).
5. G. Ricort and C. Aime, Astron. Astrophys. **76**, No. 2, 324–335 (1979).
6. G. Ricort, C. Aime, and C. Roddier, Sol. Phys. **69**, No. 2, 223–231 (1981).